Ocean Surface Wave Optical Roughness: Innovative Polarization Measurement

Christopher J. Zappa
Lamont-Doherty Earth Observatory of Columbia University
Ocean and Climate Physics Division
61 Route 9W, Palisades, NY 10964
phone: (845) 365-8547 fax: (845) 365-8157 email: zappa@ldeo.columbia.edu

Award Number: N00014-06-1-0372

LONG-TERM GOALS

We are part of a multi-institutional research team* funded by the ONR-sponsored Radiance in a Dynamic Ocean (RaDyO) program. The primary research goals of the program are to (1) examine time-dependent oceanic radiance distribution in relation to dynamic surface boundary layer (SBL) processes; (2) construct a radiance-based SBL model; (3) validate the model with field observations; and (4) investigate the feasibility of inverting the model to yield SBL conditions. The goals of our team are to contribute innovative measurements, analyses and models of the sea surface roughness at length scales as small as a millimeter. This characterization includes microscale and whitecap breaking waves.

* Prof. Michael L. Banner, School of Mathematics, The University of NSW, Sydney, Australia
Dr. Bertrand Chapron, Oceanography, IFREMER, Brest, France
Dr. Andres Corrada-Emmanuel, Physics Dept., Dept, U. Mass., Mass.
Dr. Tanos Elfouhaily (deceased) Applied Ocean Physics, RSMAS, Miami, Fl 33149 USA;
Dr. Johannes Gemmrich, Physics and Astronomy, UVic, Victoria, Canada
Russel P. Morison, School of Mathematics, The University of NSW, Sydney, Australia
Dr. Howard Schultz, Computer Vision Laboratory, Computer Science Dept, U. Mass., Mass
Dr. Christopher Zappa, Lamont Doherty Earth Observatory, Columbia Univeristy, Palisades, NY

OBJECTIVES

Nonlinear interfacial roughness elements - sharp crested waves, breaking waves as well as the foam, subsurface bubbles and spray they produce, contribute substantially to the distortion of the optical transmission through the air-sea interface. These common surface roughness features occur on a wide range of length scales, from the dominant sea state down to capillary waves. Wave breaking signatures range from large whitecaps with their residual passive foam, down to the ubiquitous centimeter scale microscale breakers that do not entrain air. There is substantial complexity in the local wind-driven sea surface roughness microstructure. Traditional descriptors of sea surface roughness are scale-integrated statistical properties, such as significant wave height, mean squared slope (eg. Cox and Munk, 1954) and breaking probability (e.g. Holthuijsen and Herbers, 1986). Subsequently, spectral characterisations of wave height, slope and curvature have been measured, providing a scale resolution into Fourier modes for these geometrical sea roughness parameters. More recently, measurements of whitecap crest length spectral density (eg. Phillips et al, 2001, Gemmrich, 2005) and microscale breaker crest length spectral density (eg. Jessup and Phadnis, 2005) have been reported.

Report Documentation Page

Form Approved
OMB No. 0704-0188

1. REPORT DATE	2. REPORT TYPE	3. DATES COVERED
2006	**N/A**	**-**

4. TITLE AND SUBTITLE	5a. CONTRACT NUMBER
Ocean Surface Wave Optical Roughness: Innovative Polarization Measurement	5b. GRANT NUMBER
	5c. PROGRAM ELEMENT NUMBER
6. AUTHOR(S)	5d. PROJECT NUMBER
	5e. TASK NUMBER
	5f. WORK UNIT NUMBER
7. PERFORMING ORGANIZATION NAME(S) AND ADDRESS(ES) **Lamont-Doherty Earth Observatory of Columbia University Ocean and Climate Physics Division 61 Route 9W, Palisades, NY 10964**	8. PERFORMING ORGANIZATION REPORT NUMBER
9. SPONSORING/MONITORING AGENCY NAME(S) AND ADDRESS(ES)	10. SPONSOR/MONITOR'S ACRONYM(S)
	11. SPONSOR/MONITOR'S REPORT NUMBER(S)

12. DISTRIBUTION/AVAILABILITY STATEMENT
Approved for public release, distribution unlimited

13. SUPPLEMENTARY NOTES
The original document contains color images.

14. ABSTRACT

15. SUBJECT TERMS

16. SECURITY CLASSIFICATION OF:			17. LIMITATION OF ABSTRACT	18. NUMBER OF PAGES	19a. NAME OF RESPONSIBLE PERSON
a. REPORT	b. ABSTRACT	c. THIS PAGE			
unclassified	**unclassified**	**unclassified**	**UU**	**10**	

Our effort seeks to provide a more comprehensive description of the physical and optical roughness of the sea surface. We will achieve this by implementing a comprehensive sea surface roughness observational 'module' within the RADYO field program to provide optimal coverage of the fundamental optical distortion processes associated with the air-sea interface. Within our innovative complementary data gathering, analysis and modeling effort, we will pursue both spectral and phase-resolved perspectives. These will contribute directly towards refining the representation of surface wave distortion in present air-sea interfacial optical transmission models.

APPROACH

We will build substantially on our accumulated expertise in sea surface processes and air-sea interaction. We are working within the larger team (listed above) measuring and characterizing the surface roughness. The group plans to contribute the following components to the primary sea surface roughness data gathering effort in RaDyO:

- *polarization camera measurements* of the sea surface slope topography, down to capillary wave scales, of an approximately 1m x 1m patch of the sea surface (see Figure 1), captured at video rates. [Schultz]

- *co-located and synchronous orthogonal 75 Hz linear scanning laser altimeter* data to provide spatio-temporal properties of the wave height field (resolved to O(0.5m) wavelengths) [Banner, Morison]

- *high resolution video imagery* to record whitecap data, from two cameras, close range and broad field [Gemmrich]

- *fast response, infrared imagery* to quantify properties of the microscale breakers, and surface layer kinematics and vorticity [Zappa]

- *sonic anemometer* to characterize the near-surface wind speed and wind stress [Zappa]

Our envisaged data analysis effort will include: detailed analyses of the slope field topography; laser altimeter wave height and large scale slope data; statistical distributions of whitecap crest length density in different scale bands of propagation speed and similarly for the microscale breakers, as functions of the wind speed/stress and the underlying dominant sea state. Our contributions to the modeling effort will focus on using the data to refine the sea surface roughness transfer function. This comprises the representation of nonlinearity and breaking surface wave effects including bubbles, passive foam, active whitecap cover and spray, as well as microscale breakers.

WORK COMPLETED

Our effort in FY07 has been primarily in the detailed planning of the suite of sea surface roughness measurements that we will undertake during the Scripps Institute of Oceanography (SIO) Pier Experiment scheduled for January 6-28, 2008. During FY07 we refined our choices of the instrumentation needed to make the measurements described in the preceding section, and continued work on the analysis techniques for characterizing the various roughness features. We participated in

the FY07 RaDyO scientific planning meetings, which were held in Montreal in October 2006 and at SIO in June 2007.

A portion of our research team, Christopher Zappa, Michael Banner, and Howard Schultz completed the analysis of a proof-of-concept study to assess the effectiveness of a new passive optical technique based on polarimetry. The Polarimetric Slope Sensing (PSS) concept exploits the scattering properties of light from the air-water boundary to recover the instantaneous two-dimensional slope field of a water surface. In principle, the polarization vector properties [polarization orientation and degree of linear polarization] of the sea surface reflection of incident skylight provide sufficient information to determine the local surface slope vector normal [Φ, Ψ] relative to the camera orientation. A controlled laboratory tank experiment was carried out with mechanically-generated gravity waves at Lamont-Doherty Earth Observatory. The second phase of this study was performed from the Piermont pier on the Hudson River, near Lamont Doherty Earth Observatory. The results discussed below are about to be submitted for publication in the next month [Zappa et al, 2007].

RESULTS

(i) Instrumentation proposed for the Scripps Institution of Oceanography pier experiment, January 6-28, 2008. The instrumentation complement that will be deployed in this filed testing phase is shown below in Figure 1.

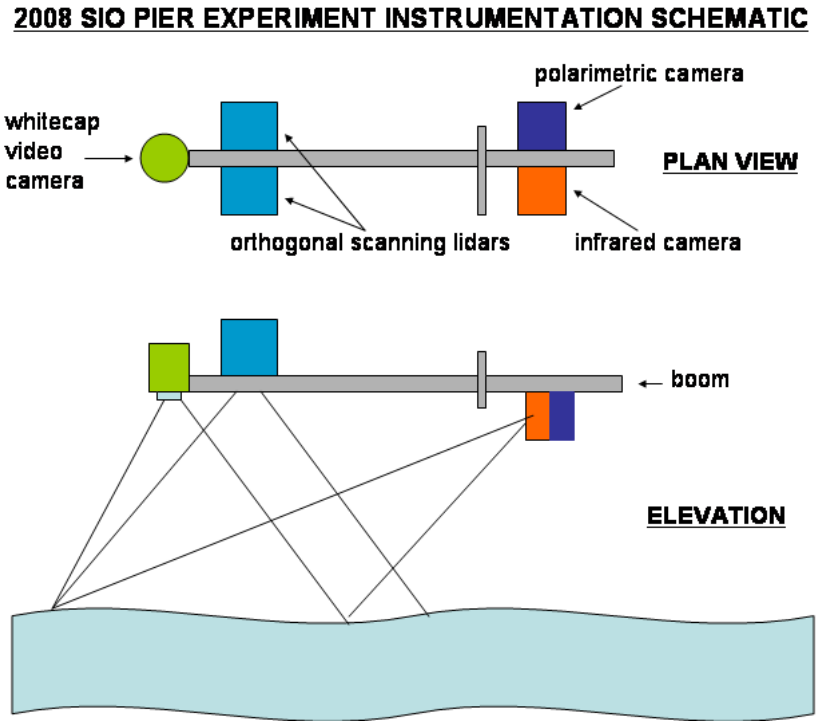

Figure 1. Schematic of instrumentation packages to be deployed from the northern swinging boom at the end of the Scripps pier. The end of the instrumentation boom will be about 9m from the edge of the pier and about 10m above the mean water level. The approximate field of view of the various instruments is shown. There is another wide angle whitecap video camera mounted well above the boom.

Banner/Morison plan to deploy two orthogonal line scanning lidars, synchronized for zero crosstalk. These will be positioned on the boom so that their intersection point is within the common footprint of the polarimetric (Schultz), infrared (Zappa) and visible (Gemmrich) imagery cameras to measure small-scale surface roughness features and breaking waves.

Zappa will deploy his infrared/visible camera system (with blackbody target, a blackbody controller, a laser altimeter). He will also deploy his environmental monitoring system (sonic anemometer, a Licor water vapor sensor, a Vaisala RH/T/P probe, a motion package, a pyranometer, and a pyrgeometer).

Gemmrich will deploy 2 video visible imagery cameras. One camera will be mounted on the main boom next to our other instrumentation packages. The second camera will be mounted higher up to provide a wider perspective on larger scale breaking events.

Schultz/Corrada-Emmanuel will deploy an instrument package located on the boom that includes a polarimetric camera imaging the very small-scale waves, an autofocus controller for this camera, a laser rangefinder for the autofocus mechanism, a polarimetric camera looking up at the sky and a motion package.

The individual data acquisition systems will be synchronized to GPS accuracy so that the various data sets can be interrelated.

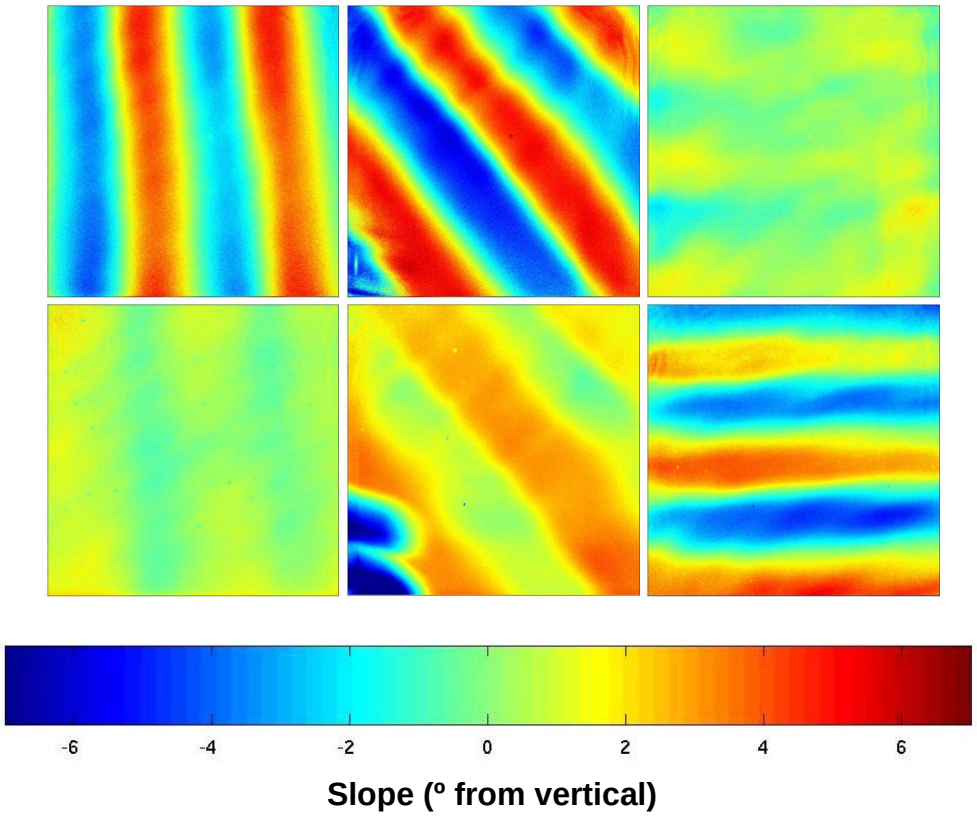

Figure 2. Polarimetric image frame pairs from 3 laboratory experimental runs showing the slope of the water surface. For each pair, the image on the top is the x-direction (cross-look-direction) slope and the image on the bottom is the y-direction (look-direction) slope. The left pair is for the camera look direction perpendicular to the wave propagation direction. The middle pair from the top is for the camera look direction 45º to the wave propagation direction. The right pair is for the camera look direction into the wave propagation direction. Note that the distortion in the lower left corner of the 45º case is due to a polarized reflection that affects the slope. This region is not considered in subsequent analysis. The field-of-view in all images is roughly 12.9cm x 16.8cm.

(ii) A technical evaluation of the PSS technique requires a comparison of the surface wave field as determined by the polarimetric data with that from a robust in-situ wave gauge. Figure 2 shows the slope imagery from the linear wave slope cases perpendicular to wave propagation, oblique to wave propagation (45º), and parallel to wave propagation. Several movies of the experimental runs are available for download from our website: http://www.ldeo.columbia.edu/~felixt/polarization/. For all Cases, the mean wavelength determined from zero-crossings in the slope imagery was 6.42 ± 0.66 cm and the dominant wavelength determined in the wave spectrum was 6.63 ± 0.53 cm. A direct comparison of the wave slope determined from the polarimetric imagery and in-situ wire wave gauge is made in Figure 3. This figure shows the total RMS wave slope from the polarimetric imagery versus the RMS wave slope determined from $1/C * \partial\eta/\partial t$ described above. The total slope at each pixel is defined by $\sqrt{S_x^2 + S_y^2}$ where S_x and S_y are the x- and y-components of slope, respectively. The mean slope for the ensemble of images during a run is removed and the total RMS wave slope is computed using all pixels in all images in that run. For a given incidence angle and azimuth, the results show a strong sensitivity to the known wave slope in each azimuth orientation. For uniform unpolarized

incident lighting, this sensitivity should be the same and in 1:1 agreement with no azimuthal dependence. This was confirmed in Figure 3. Potential sources for the variability in Figure 3 are: the polarimetric camera calibration, the variation in distance of the bore-sighted imagery from the wave generator and across the tank, and any non-uniformity in the background incident polarized light. The first two sources have been estimated and their associated uncertainties are shown in Figure 3. The non-uniformity of background incident polarized light is not precisely known, but believed to be minimal based upon surveys with an instrument that can only detect significant polarization gradients. The coefficient of determination for the results in Figure 3 is 0.98. This demonstrates that the slope results from the polarimetric camera provide a robust characterization of the repeatable short quasi-sinusoidal gravity wave system.

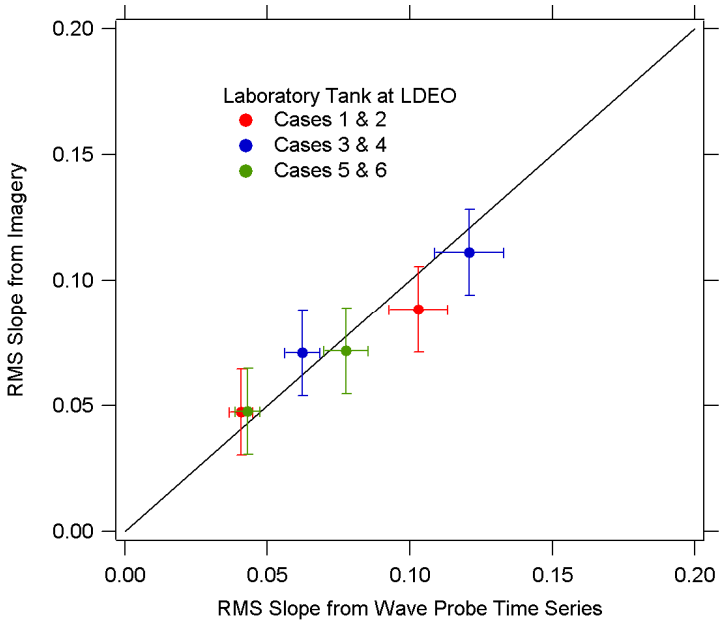

Figure 3. Total RMS wave slope from the polarimetric imagery versus the total RMS wave slope determined from the in-situ wave probe. Uncertainty bounds show the variability in the polarimetric camera calibration and the wave slope variability in the tank at the known image locations. Cases 1 & 2 are for the camera look direction perpendicular to the wave propagation direction, Cases 3 & 4 are for the camera look direction 45° to the wave propagation direction, and Cases 5 & 6 are for the camera look direction into the wave propagation direction.

Following the success of the laboratory phase in delivering robust, reliable slope field data, we performed a field experiment at the Piermont Pier. Slope imagery (x and y components) from the field is shown in Figure 4. The top pair is the raw image slope as determined from the polarimetric camera. The slope arrays produced from the field experiments showed a bias in the form of a non-zero temporally-averaged slope. The bias was estimated by averaging each pixel over all frames. The exact cause of the slope bias is under investigation, but may have been caused by sky conditions or errors in estimating the camera viewing angle. The bottom pair has the image bias removed using a temporal reconstruction, i.e., the bias image was subtracted from each individual slope image. The comparison of the two pairs shows the distinct bias due to non-uniformities in the reflected polarization signal from the background sky. This suggests that an upward-looking camera would provide the information necessary to correct for reflected polarized radiation. The water surface structure shows short wind

waves of *O* (10 cm) wavelength propagating across the image from left to right. The structure of the wind-roughened surface is similar to that observed in the laboratory. Another time series of slope imagery (x and y) at the Piermont Pier is shown in Figure 5. The image time series shows the passage of one breaking wave in the lower portion of the image and a second wave beginning to break in the upper left portion. Both breaking waves that propagated through the sequence had a wavelength of *O*(1 m). In this case, the fine-scale structure of the breaking crest and its wake left behind are captured without blurring by the polarimetric camera. The wind-roughened surface observed in Figure 5 was not observed and longer gravity waves of *O*(10 cm – 1 m) had developed.

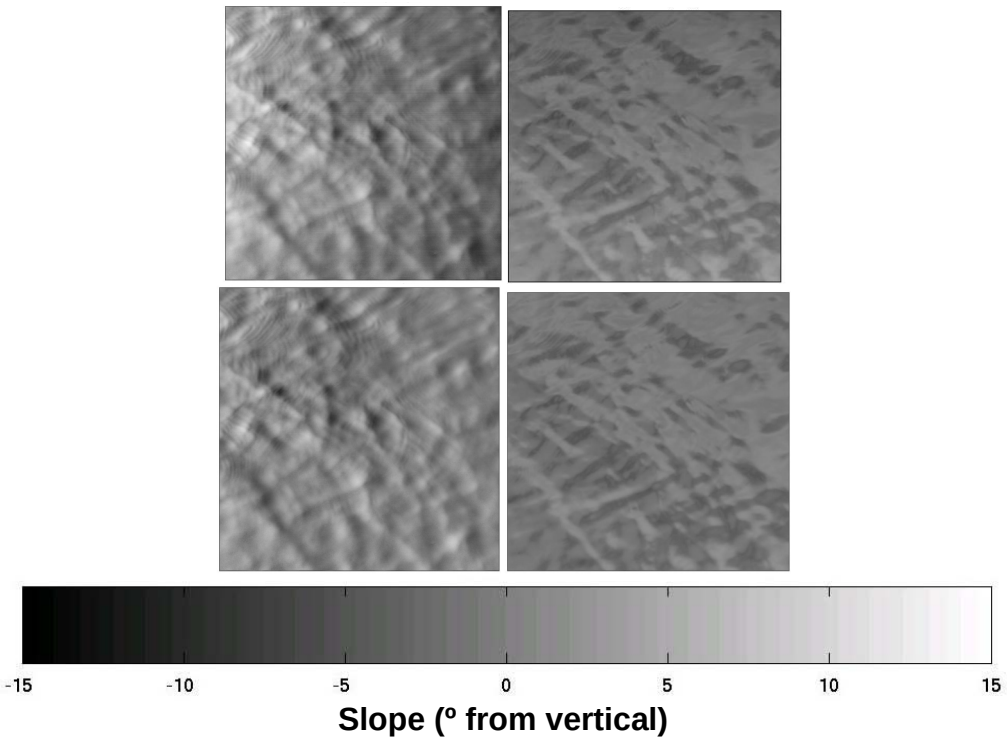

Figure 4. Polarimetric image frame pairs from Run 4 of the Piermont Pier experiment showing the slope of the water surface. For each pair, the image on the left is the x-direction (cross-look-direction) slope and the image on the right is the y-direction (look-direction) slope. The top pair is the raw image slope as determined from the polarimetric camera. The bottom pair has the image bias removed using a temporal reconstruction. The field-of-view in all images is roughly 1.3m x 2.6m.

A direct comparison of the wave slope on the Hudson River determined from the polarimetric imagery and Rigel laser altimeter is made in Figure 6. Figure 6 shows the total RMS wave slope from the polarimetric imagery versus the RMS wave slope determined from $1/C * \partial\eta/\partial t$ using the laser altimeter. Slope statistics are computed over the region of the image equivalent to the effective Riegl laser altimeter field-of-view. Note that small boats passing caused waves that propagated into the image field-of-view in addition to the existing surface waves on the Hudson River. The dominant waves were of the same scale as the image size. The frequency of the dominant waves determined from time series of the wave slope imagery and of the Riegl laser altimeter were the same and ranged from 0.45 Hz to 0.72 Hz for the data conditions presented in the field. The coefficient of determination for the results in Figure 6 is 0.98 and demonstrates that the slope results from the polarimetric camera

are a robust characterization of the fine-scale surface roughness features that are intrinsic to wind-driven air-sea interaction processes.

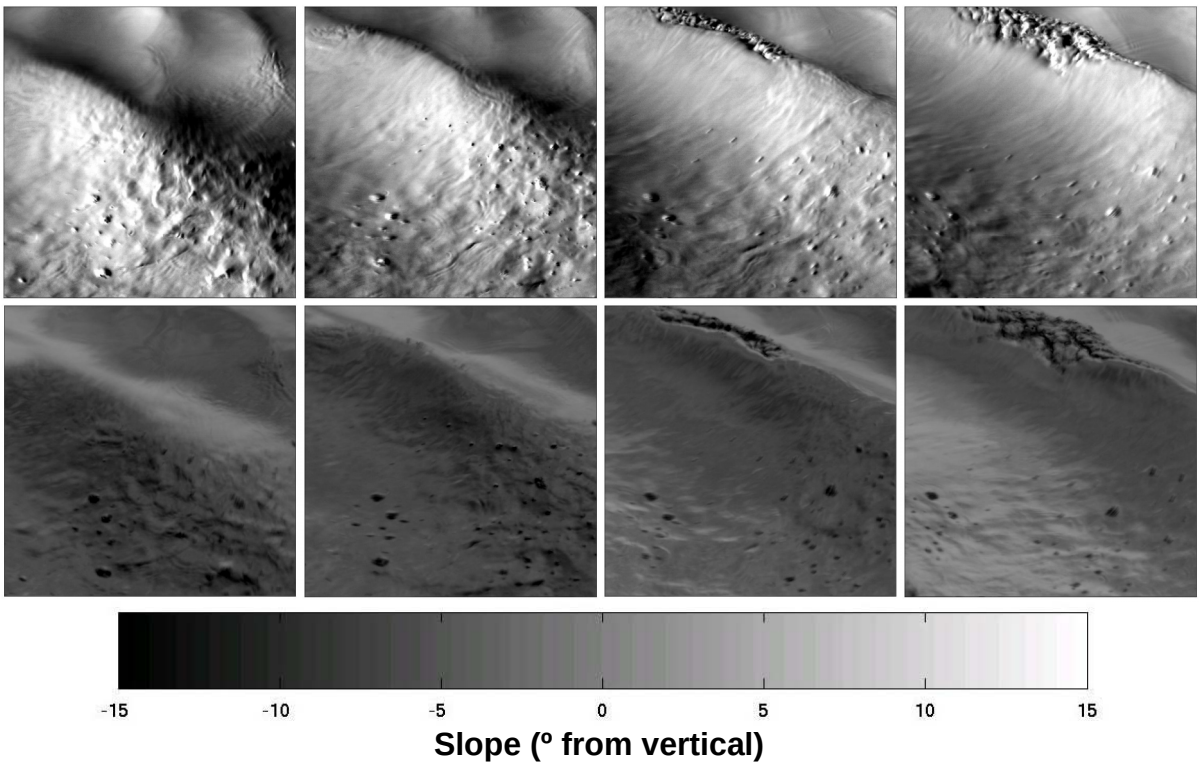

Figure 5. ***Polarimetric image frame time series with the bias removed during the Piermont Pier experiment showing the slope of the water surface at the completion of one breaking wave and as a second wave begins to break. The images on the top are the x-direction (cross-look-direction) slope and the images on the bottom are the y-direction (look-direction) slope. The field-of-view in all images is roughly 1.3m x 2.6m. The images are separated by 0.13 s. The slope is computed as the specular angle greater than or equal the Brewster angle.***

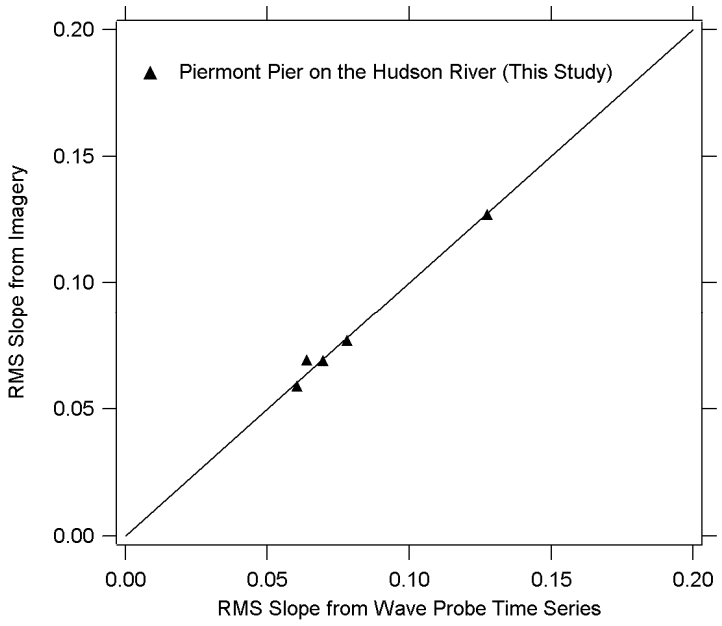

Figure 6. Comparison of polarization camera and laser altimeter results. Scatter plot of the total root mean-squared slope from the polarimetric imagery versus the total root mean squared wave slope from the laser altimeter during the field experiment at Piermont Pier on the Hudson River.

IMPACT/APPLICATIONS

This effort will provide a far more detailed characterization of the wind driven air-sea interface, including wave breaking (whitecaps and microscale breaking). This is needed to provide more complete parameterizations of these processes, which will improve the accuracy of ocean optical radiative transfer models and trans-interfacial image reconstruction techniques.

The PSS concept here will allow the research team to pursue the application of an operational, field-deployable polarimetric imaging system for recovering the two-dimensional time-varying slope field of short gravity waves at video frame rates. Our vision is to develop optical polarimetry as a primary tool for measuring the small-scale sea surface features responsible for the optical distortion processes associated with the air-sea interface. Within our innovative complementary data gathering/analysis/modeling effort, we will have a leading edge capability to provide both spectral and phase-resolved perspectives. These will contribute directly towards our effort within the RaDyO DRI to refine the representation of surface wave distortion in present air-sea interfacial optical transmission models.

RELATED PROJECTS

The results here led to a DURIP award (H. Schultz, U. Mass.) for a PSS system that will spark a new class of instrumentation that will benefit a wide variety of oceanography and fluid mechanics research and educational programs. The DURIP will contribute PSS directly towards our effort within the ONR RaDyO DRI scheduled for FY07-10 and will provide a much-needed refinement in the representation of surface wave distortion in present air-sea interfacial optical transmission models.

The work here is a direct follow-on from the Waves, Air-Sea Fluxes, Aerosols, and Bubbles (WASFAB) experiments in 2005 at the FRF pier in Duck, NC. The results from WASFAB will directly augment the capabilities for quantification of the distribution of microscale wave breaking and whitecapping in the understanding of air-sea interaction.

REFERENCES

Cox, C.S. and Munk, W.H., 1954: Measurements of the roughness of the sea surface from photographs of the sun glitter. *J. Opt. Soc. Am*. 44, 838-850.

Gemmrich, J, 2005: 'On the occurrence of wave breaking', *14th 'Aha Huliko'a Hawaiian Winter Workshop*, January 2005, Proceedings, Eds. P. Muller et al., 123-130.

Holthuijsen, L.H., and T.H.C. Herbers, 1986: Statistics of breaking waves observed as whitecaps in the open sea, *Journal of Physical Oceanography*, 16, 290-297.

Jessup, A.T. & Phadnis, K.R. 2005 Measurement of the geometric and kinematic properties of microsacle breaking waves from infrared imagery using a PIV algorithm. *Meas. Sci. Technol.* 16, 1961-1969.

Phillips, O. M., Posner, F. L., and Hansen, J. P. 2001 High resolution radar measurements of the speed distribution of breaking events in wind-generated ocean waves: surface impulse and wave energy dissipation rates. *J. Phys. Oceanogr.*, 31, 450–460.

Zappa, C.J., M.L. Banner, H.J. Schultz, A. Corrada-Emmanuel, L.B. Wolff, & J. Yalcin, 2007, Polarization imagery of a water surface for short ocean wave slope retrieval, *Measurement and Science Technology*, submitted.